Non-axisymmetric turbine end wall profiling

D G Gregory-Smith[1*], **G Ingram**[1], **P Jayaraman**[2], **N W Harvey**[3] and **M G Rose**[3]
[1]School of Engineering, University of Durham, UK
[2]School of Chemical Engineering, University of Birmingham, UK
[3]Rolls–Royce plc, Derby, UK

Abstract: A design method for profiling the end wall to reduce secondary flow has been reported previously. A profile has been tested in the Durham Linear Cascade and the results confirmed the design method. This paper describes the design and testing of a second-generation end wall, where the profiling is more suited to a real turbine. The new end wall has been tested in the linear cascade and a comprehensive set of measurements have been taken. These include traverses of the flow field upstream and downstream of the blade row, surface static pressure distributions on the end wall and flow visualization. Comparisons have been made with the results with a planar end wall and the earlier profiled end wall. Observed reductions in exit angle deviations are even greater than for the first design, although the loss reduction is not as great. The results verify the design, confirming profiled end walls as a means of reducing secondary flow, kinetic energy and loss. Overall an improved understanding of the effects of end wall profiling has been obtained although further work is required in this area.

Keywords: turbines, turbomachinery, end walls, profiling, non-axisymmetric, secondary flow

NOTATION

C_{PS}	static pressure coefficient
P0	label for planar end wall
P1	label for first-generation profiled end wall
P2	label for second-generation profiled end wall
PS	pressure side
SS	suction side

1 INTRODUCTION

Turning the sheared flow due to the hub or casing boundary layers at inlet to a blade row causes secondary flows to be produced. In essence, the cross-passage pressure gradient set up by the mainstream flow sweeps the low momentum boundary fluid from pressure to suction surface on the end wall, with a compensating counterflow at a distance from the wall. Other phenomena are associated with secondary flow, which has been studied extensively and of which a comprehensive review was made by Sieverding [**1**]. The secondary flow gives rise to increased loss within the blade row and produces a non-uniform flow at exit which may cause extra loss in succeeding blade rows.

In a low aspect ratio highly loaded turbine, the effects of secondary flow are evident throughout most of the flow field, and the secondary loss may account for about half of the total loss. A widely used method of reducing secondary flows is to use non-radial stacking or blade lean which aims to unload the blade end, thus reducing the cross-passage pressure difference there, as described by Harrison [**2**]. Profiling of the end wall(s) of a blade row also holds promise for reducing secondary flow through the reduction of the cross-passage pressure difference at the end wall. This could be used in addition to blade lean or where blade lean is not desirable, as in a stressed rotor blade. A number of workers have tried various profiles, for instance Deich *et al.* [**3**] and Morris and Hoare [**4**] in linear cascades and Ewen *et al.* [**5**] and Boletis [**6**] in rotating rigs. Generally some improvements have been reported, but the results are rather variable. With the advent of computational fluid dynamics (CFD) some workers have used a more systematic approach using CFD to help to design profiles, for instance Atkins [**7**] and Rose [**8**]. Rose used a CFD method to design a non-axisymmetric end wall profile to reduce the non-uniformity of static pressure distribution at the platform edge downstream of the trailing edge of nozzle guide vanes. The object was to reduce the cooling air flow requirements to avoid hot gas ingestion. Hartland *et al.* [**9**] used Rose's idea to design a non-axisymmetric

This paper was presented at the 4th European Conference on 'Turbomachinery' held in Firenze, Italy on 20–23 March 2001. The MS was received on 17 May 2001 and was accepted after revision for publication on 14 June 2001.
**Corresponding author: School of Engineering, University of Durham, South Road, Durham DH1 1LE, UK.*

end-wall profile for a row of rotor blades and showed that the method worked well when tested in linear cascade. They also showed that there was a significant effect on the secondary flow. The profile had convex curvature on the end wall near the pressure surface, reducing the pressure there, and concave curvature near the suction surface, raising the pressure there. Thus the cross-passage pressure gradient was reduced, reducing the secondary flow. This principle was also used by Yan *et al.* [**10**] to reduce the secondary flows in a nozzle row of a steam turbine.

Harvey *et al.* [**11**] described an inverse design method for end wall profiles to reduce secondary flow. This method made use of a CFD code based on the method described by Moore [**12**]. The code uses the pressure correction algorithm and a mixing length type turbulence model with wall functions. A computation uses typically 100 000 grid points for the half-span. This modest number of points is adequate for this application without the need for a low Reynolds number turbulence model. The computation of the secondary flow is expected to be good, although the loss prediction less accurate. Hartland *et al.* [**13**] tested in a linear cascade a profile designed by the method to provide experimental verification. The profile (known as P1) tested by Hartland *et al.* extended some distance upstream and downstream of the blade row, and so was not suitable for application to a real machine. The object of the work reported in this paper was to use the inverse design method to produce a second profile (known as P2) restricted to the blade passage. The axial restriction could result in a more 'extreme' profile with sharper differences in curvature. Thus it was important to provide an experimental test for such a profile. It should be mentioned that the inverse design method was based on reducing the secondary flow, as this is likely to be more reliably predicted than loss by the CFD method. Thus it is important to carry out experimental investigations to ascertain the extent to which reductions in secondary flow result in reductions in loss.

2 EXPERIMENTS

2.1 Durham cascade

The cascade contains rotor blades with an inlet angle (from axial) of 42.75° and an exit angle of −68.7°; these are similar to those of a high pressure axial flow turbine. The axial chord is 181 mm and the half-span 200 mm. The flow is low Mach number and upstream there is a grid of bars to raise the inlet turbulence intensity to ∼5 per cent. The cascade geometry is described in detail by Gregory-Smith and Cleak [**14**].

The instrumentation included end wall static pressure tappings in order to determine the effect of the profile on the pressure distribution which drives the secondary flow. There are slots in one end wall through which probes can be inserted to measure the flow in the opposite half-span. Five-hole pressure probes were used to determine the inlet flow and the flow at exit at a plane 28 per cent axial chord downstream (known as slot 10). A full description of these measurements is given by Jayaraman [**15**]. In addition extensive surface flow visualization was carried out with an oil and dye mixture in order to investigate the flow on the end wall and suction surface.

2.2 End wall profile design

The design of profile P2 was carried out using the inverse method described by Harvey *et al.* [**11**], although it has been somewhat developed since that paper was published. As mentioned above, the profiling of P2 was restricted to the blade passage region, unlike P1. A further difference was that P1 had a ridge extending downstream which enhanced the countervortex, since the design intent had been to reduce the overturning (see Hartland *et al.* [**13**]). As this vortex will result in increased mixing loss, this ridge was eliminated. The manufacture of the end wall and the insertion of the static pressure tappings are described by Jayaraman [**15**].

Figure 1 shows a photograph of the end wall profile P1 and Fig. 2 shows P2, both taken from upstream. For both P1 and P2, the convex curvature near the pressure surface (to reduce static pressure) can be seen as can also the concave curvature near the suction surface (to raise the pressure). P1 shows the profiling extending some distance upstream in the form of a ridge from near the pressure surface. Further details of P1 are given by Harvey *et al.* [**11**]. However, for P2, the restriction in the axial extent of the profile results in a high concave curvature near the pressure side of the leading edge.

3 RESULTS

3.1 End wall static pressures

Figure 3 shows the contours of static pressure coefficient (referenced to inlet conditions) for the planar end wall, profile P1 (taken from reference [**13**]) and profile P2. It may be appear that the periodicity is not perfect, but this is an artefact of the contour plotting program. Hartland *et al.* [**13**] indicate a reasonable degree of periodicity. The effect of the profiling may be seen if, for instance, the −1.0 contour is followed. For the three end walls it leaves the pressure side at about −30 mm axial position. For the planar wall it goes across the plotting area, leaving it at the 195 mm circumferential position, and coming back at 165 mm to meet the suction surface just downstream of the leading edge. However, for profile P1 the contour curves round and meets the suction surface much further downstream, at about −150 mm axial position. For P2 the

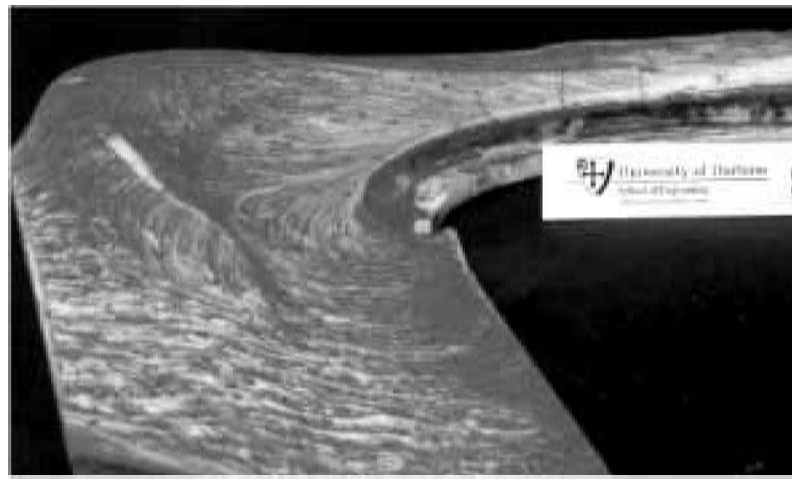

Fig. 1 Profile P1

contour goes straight across the end wall to meet the suction surface at −70 mm axial position. Thus near the suction surface, the pressure has been raised significantly. The effects of curvature on the static pressure magnitude are much greater near the suction surface because the velocity is higher there.

It may be noted that the planar end wall and P1 show some similarity in the static pressure distributions but P2 does not. Notable differences in the features are as follows:

1. P2 is seen to reduce the cross-passage pressure gradient the most. For instance at an axial position of −120 mm the change in static pressure coefficient (PS –SS) is as follows: planar, $\Delta C_{PS} \approx 2.5$; P1, $\Delta C_{PS} \approx 1.8$; P2, $\Delta C_{PS} \approx 1.0$.
2. The peak pressure for P2 is not on the pressure surface on the blade but some 20 mm away from it in the circumferential direction.
3. With P2 there is a trough in static pressure located at some distance from the suction surface, unlike the planar end wall and P1.
4. For P2 in the later part of the passage the pressure gradient is along the passage; for planar end wall and P1 the pressure gradient is inclined towards the suction surface.

3.2 Traverse results, 28 per cent axial chord downstream

The results of the five-hole probe traversing at the downstream plane, slot 10, are presented here, again making use of data from Hartland *et al.* [**13**]. Figure 4 shows the secondary velocity vectors for the planar, P1 and P2 end walls. Both P1 and P2 show a significant reduction in the main vortex, the clockwise passage vortex. In addition P2 shows a small countervortex on the wall (−300 to

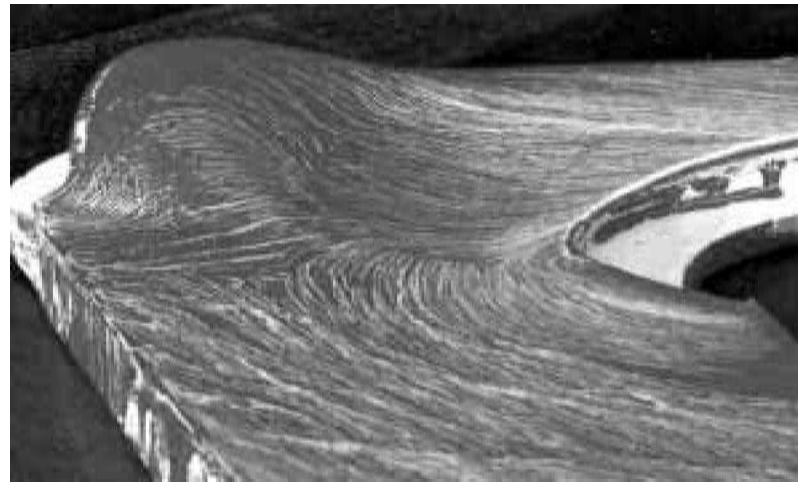

Fig. 2 Profile P2

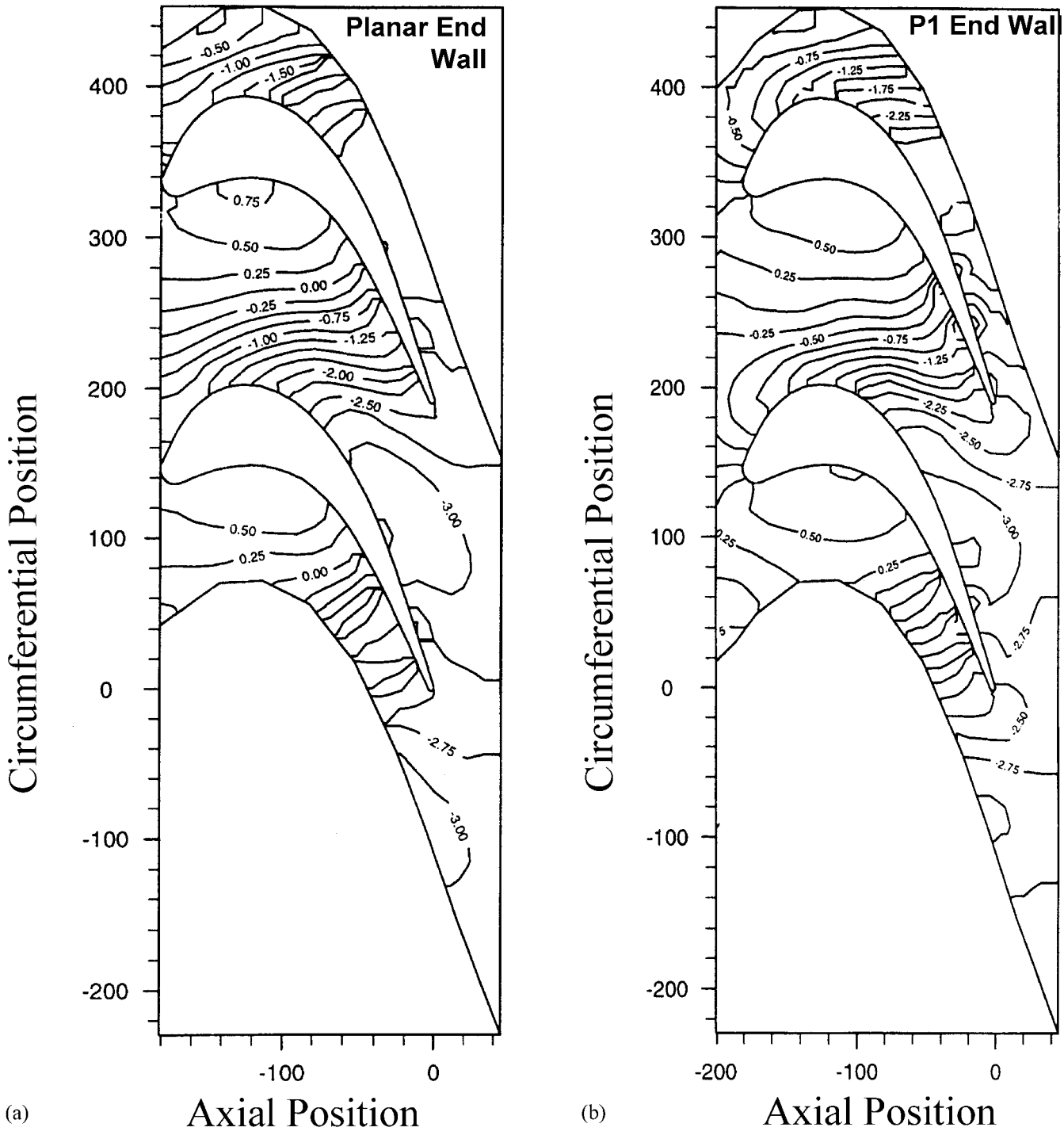

Fig. 3 (continued over)

−325 mm), similar to the planar end wall, so that the enhanced countervortex caused by the ridge in P1 has been ameliorated. Figure 5 shows the pitchwise averaged secondary kinetic energy at slot 10. The big reduction in the passage vortex with both profiles is clear. As well as being reduced, the vortex is brought closer to the end wall. However, the passage vortex strength appears a little higher for P2 than P1. Nearer the end wall, the strong countervortex with P1 has been considerably reduced with P2, although not to quite the level of the planar end wall. Figure 6 shows the variation in yaw angle for the three end walls resulting from the secondary flow. With the reduction in passage vortex strength, the under and over turning in the region of the vortex has been reduced, with P2 showing the least variation. Nearer the end wall, P2 gives rather less overturning, although

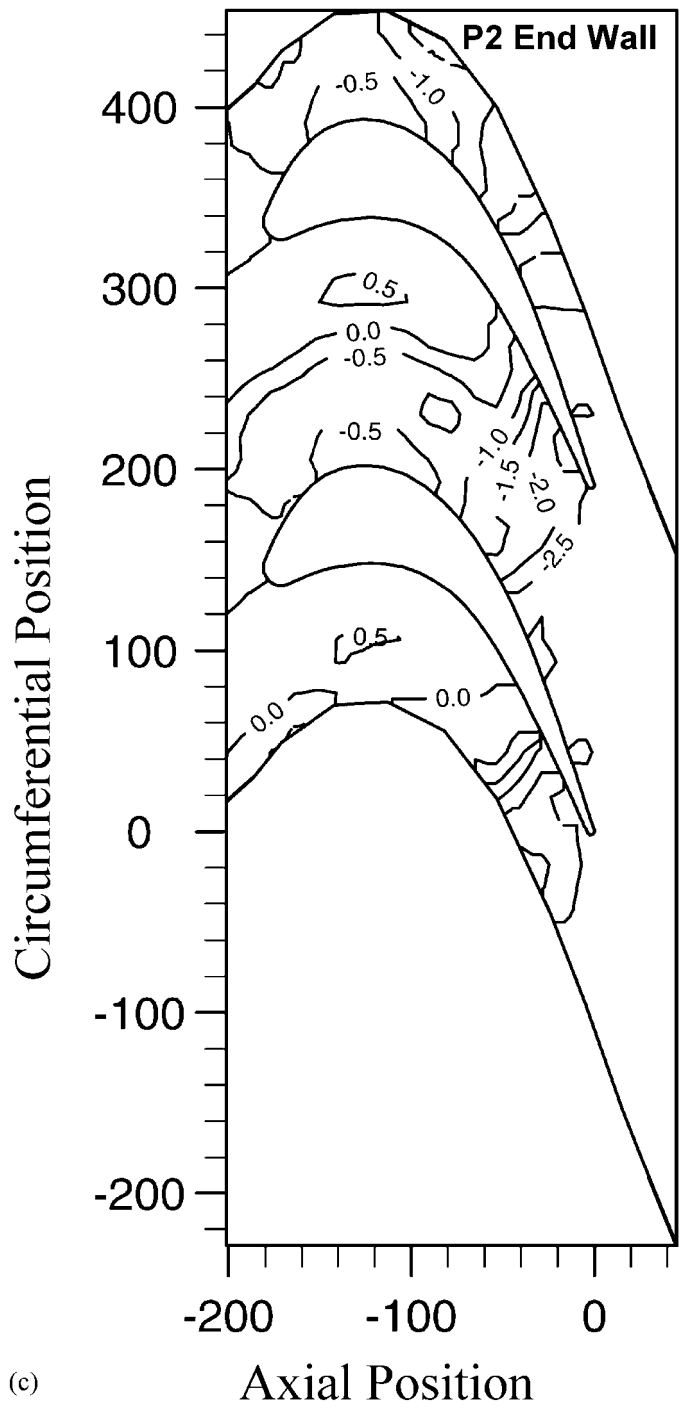

(c)

Fig. 3 End wall static pressure coefficients for (a) planar, (b) P1 and (c) P2 profiles

close to the wall the three end walls give the same overturning value. Also shown in Fig. 7 is the CFD design prediction for the yaw angle. At mid-span there is about 1.5° difference, and a similar difference was reported by Hartland *et al.* [**13**] for the planar end wall. Allowing for this, CFD and experiments agree well for the under turning peak from 120 to 40 mm from the end wall, although the slightly lower under turning for the P2 experiment is not shown by CFD. Closer than 20 mm to the end wall CFD for P1 shows much less overturning as a consequence of the strong countervortex. This is not shown by the experiments, but the resolution of the traversing is not fine enough to draw definite conclusions.

The contours of total pressure loss coefficient for the three end walls are shown in Fig. 8. The main loss core situated some distance from the end wall is caused by the action of the passage vortex sweeping up the inlet boundary layer and causing extra loss by interaction with

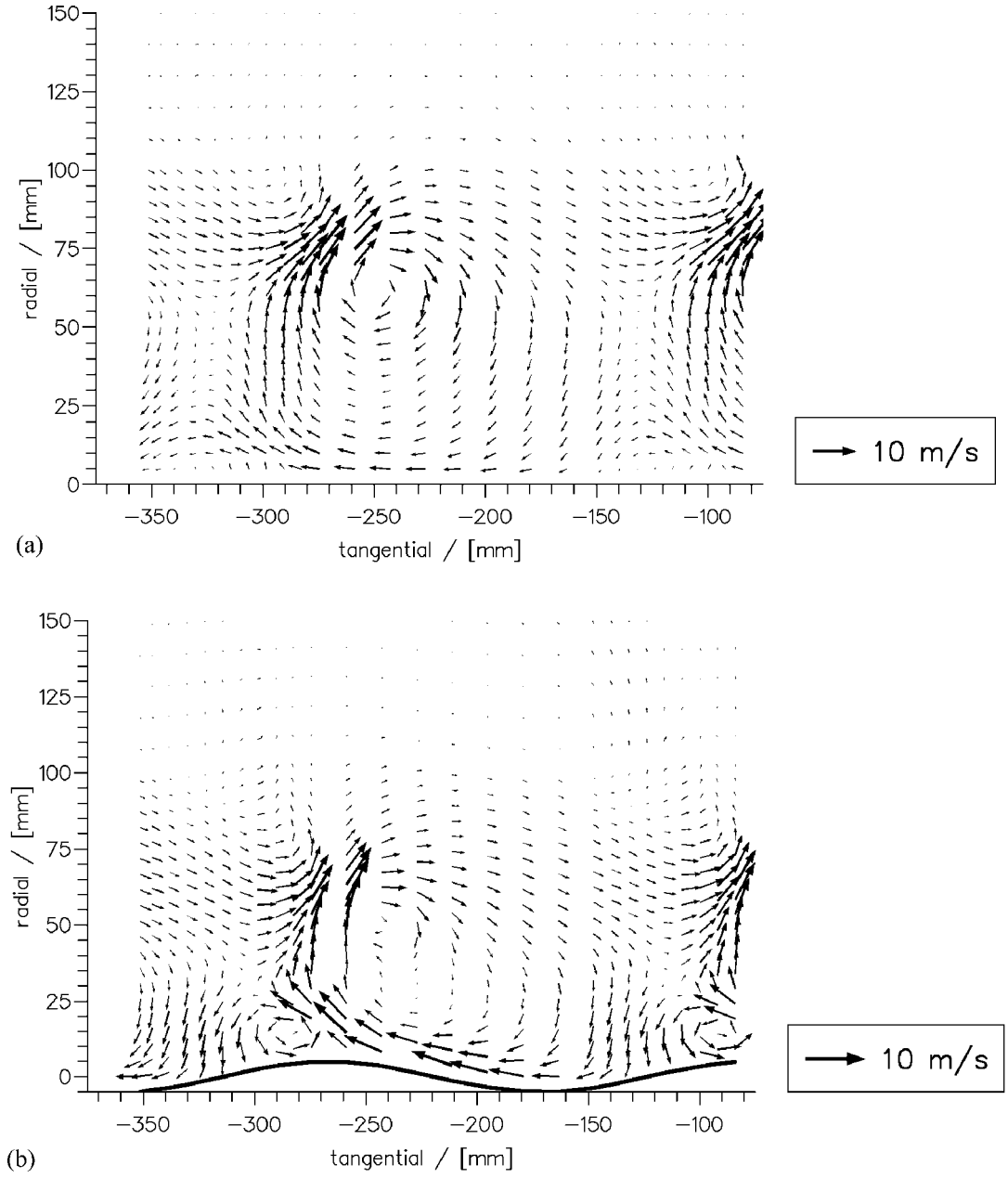

Fig. 4 (continued over)

the end wall and suction surface. For P1 and P2 the loss core is reduced in extent although the peak values (∼0.9) are similar when compared with the planar wall. A major difference between P1 and P2 is the much smaller loss associated with the countervortex in the latter, and this is expected because the countervortex has been reduced (Fig. 4). Pitch-averaged loss values are shown in Fig. 9. The main loss core is not reduced as much for P2 as it is for P1 when compared with the planar end wall. However, it is closer to the end wall corresponding to the position of the passage vortex (Figs 4 and 5). Closer to the end wall (less than 30 mm) P2 shows the reduction in loss from the countervortex compared with P1. Figure 10 shows the CFD predictions for P1 and P2. The levels are much higher with the mid-span (profile) loss being about twice the experimental value. However the prediction for P2 does show a larger loss core than for P1, as shown by the experiment. Qualitatively nearer the wall the prediction for P2 is quite good, but P1 shows a much higher loss due to the countervortex than is shown by the experiment.

3.3 Mass-averaged values at slot 10

A further quantitative picture of the effects of the end wall profiling is obtained by mass averaging the secon-

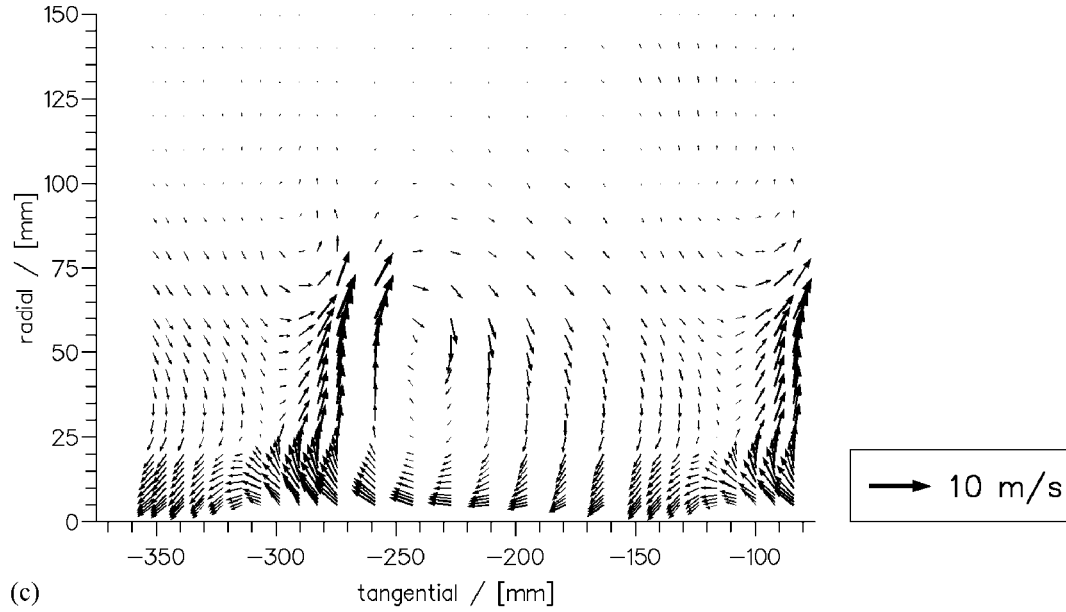

Fig. 4 Secondary velocities downstream at slot 10 for (a) planar, (b) P1 and (c) P2 profiles

dary kinetic energy and the total pressure loss over the plane of slot 10. Figure 11 shows the secondary kinetic energy, and it can be seen that overall P2 achieves almost as much reduction from the planar end wall as does P1. This agrees with the observations of the previous Figs 3 and 4.

The area-averaged loss values are shown in Fig. 12, where net values are shown, that is after subtracting the inlet loss. Two sets of values are shown; the actual values at slot 10 and the values after performing a mixing calculation to give uniform flow, the mixed-out loss. It can be seen that, in terms of loss, P2 does not perform as well as P1. The actual value is not much reduced from the planar end wall value. However the mixed-out loss value is closer to the P1 value.

3.4 Flow visualization results

End wall flow visualization was carried out on all three end walls and the blade suction surface. Presented here are views of the end walls only since the suction surface pictures are fairly similar. Figure 13 shows the flow visualization for the planar end wall, and this is quite similar to those obtained by Cleak [**16**]. The familiar features of the suction side and pressure side legs of the

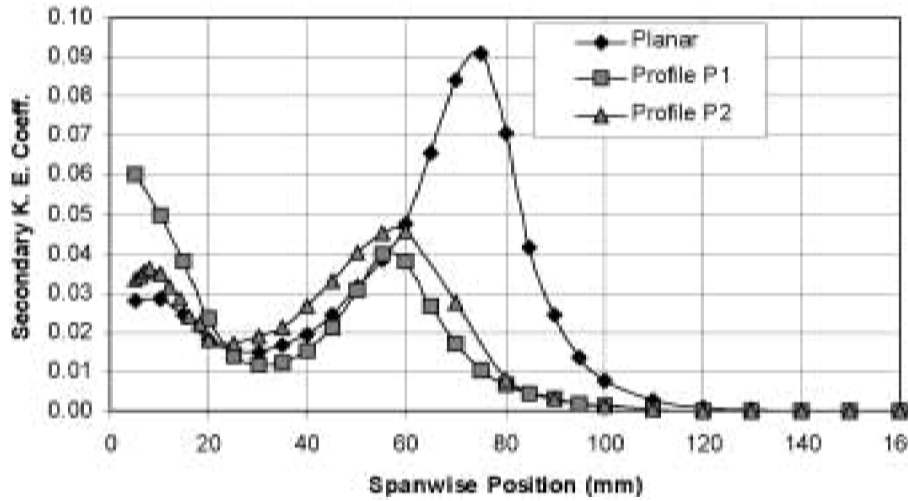

Fig. 5 Pitch-averaged secondary kinetic energy

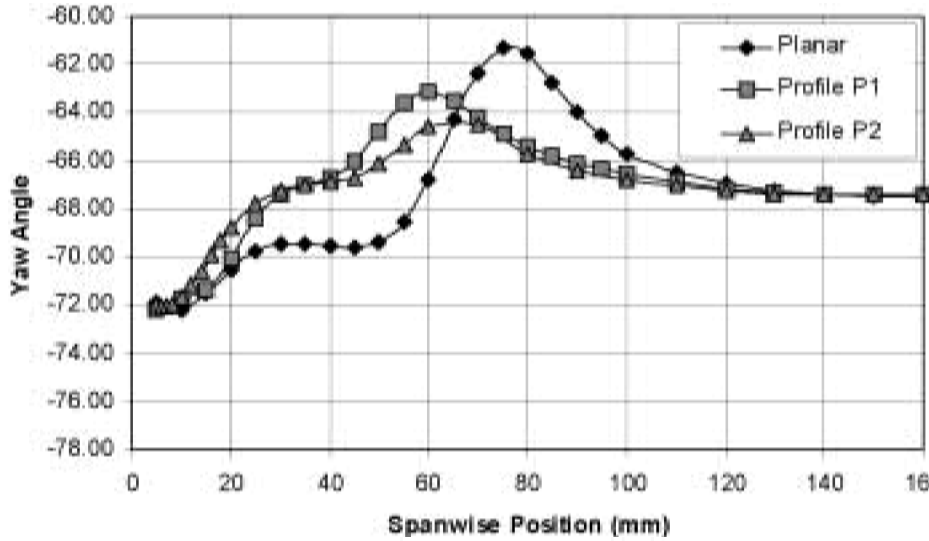

Fig. 6 Pitch-averaged yaw angle

horseshoe vortex (HSV) are clear as well as the countervortex in the end wall suction surface corner. The highly skewed new boundary layer on the end wall downstream of the pressure side leg of the HSV is flowing strongly toward the suction surface.

The flow visualization on the profiled end wall P1 is shown in Fig. 14 and also in Fig. 1. A number of differences are apparent. The two legs of the HSV appear to be less strong, particularly the pressure side leg, which is hardly distinguishable. The countervortex is still strongly visible and this is to be expected as the traverse data show this to be enhanced for P1 owing to the ridge extending downstream. The skewed new boundary layer appears to be flowing less strongly towards the suction surface. However, the most noticeable feature is a region of stagnant flow situated upstream of the leading edge on its pressure side. Figure 1 shows this to be located on the ridge extending upstream.

The flow visualization for the profiled end wall P2 is shown in Fig. 15. The flow appears to be similar to that of P1, apart from the absence of the stagnant region upstream of the leading edge. There is no evidence of separation due to the high curvature on the pressure side of the leading edge (see Fig. 2), although Jayaraman [**15**] observed highly fluctuating flow in that region when investigating the flow with tufts of cotton.

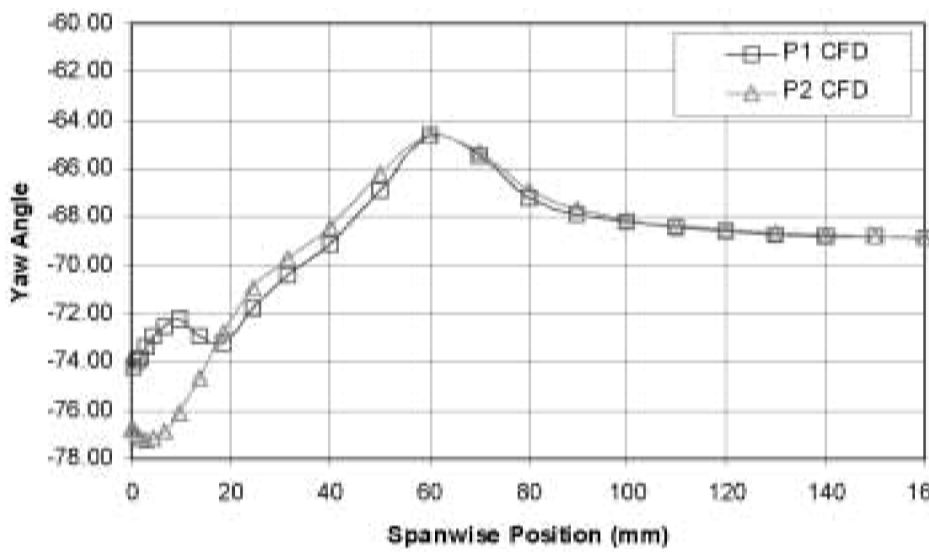

Fig. 7 CFD yaw angle predictions

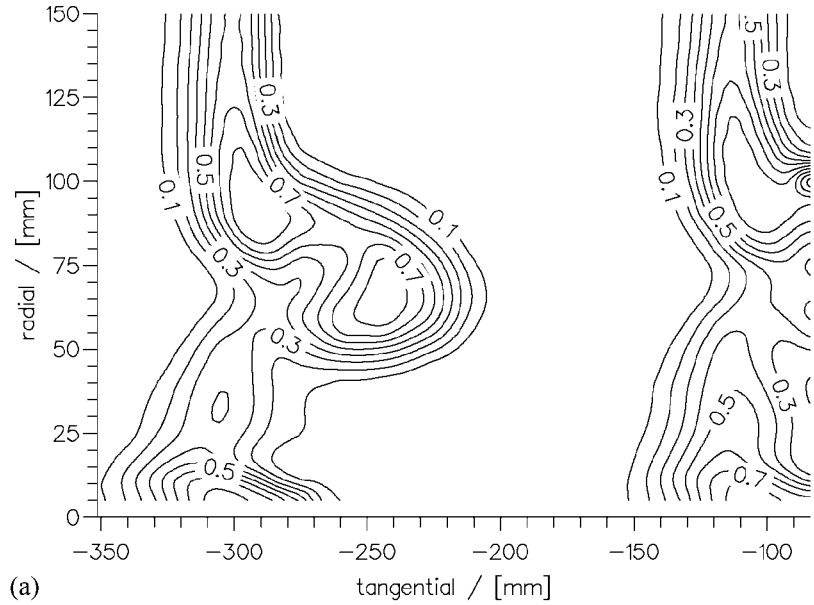

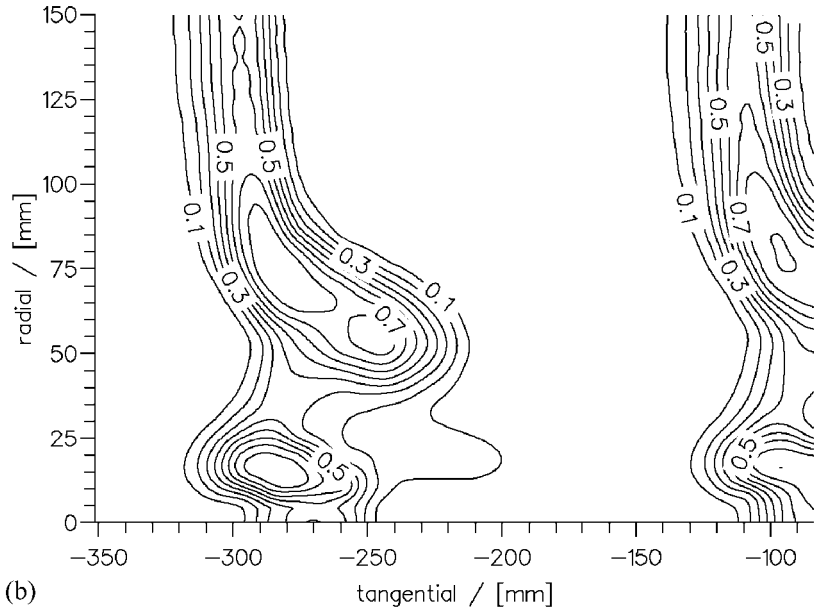

Fig. 8 (continued over)

4 DISCUSSION

Compared with the planar end wall, the end wall profiles P1 and P2 both reduce significantly the secondary flow, in particular the passage vortex. Comparing P1 and P2, the static pressure profiles on the end wall indicate that P2 has a lower cross-passage difference, so this might be expected to give a lower cross-flow on the end wall. However, neither the traverse results nor the end wall flow visualization indicates much reduction. There is slightly less overturning as the end wall is approached for P2, although the near-wall values appear similar for P1 and P2 (Fig. 6). With P2 there is a significant reduction in the countervortex which is seen in the vector plots and the loss contours in that region.

The surprising result from the P1 end wall flow visualization is the region of stagnant flow upstream of the pressure side of the leading edge (Figs 1 and 13). This is not seen with the planar end wall (or in other research workers' studies) and, although a small area was occasionally seen with P2 (Fig. 15 does not show it), an explanation was not immediately evident. So the CFD results for P1 were studied, and Fig. 16 shows the end wall streak lines. It can be seen that there is a region where no end wall flow reaches the position where the stagnant region was observed. It appears that the end wall

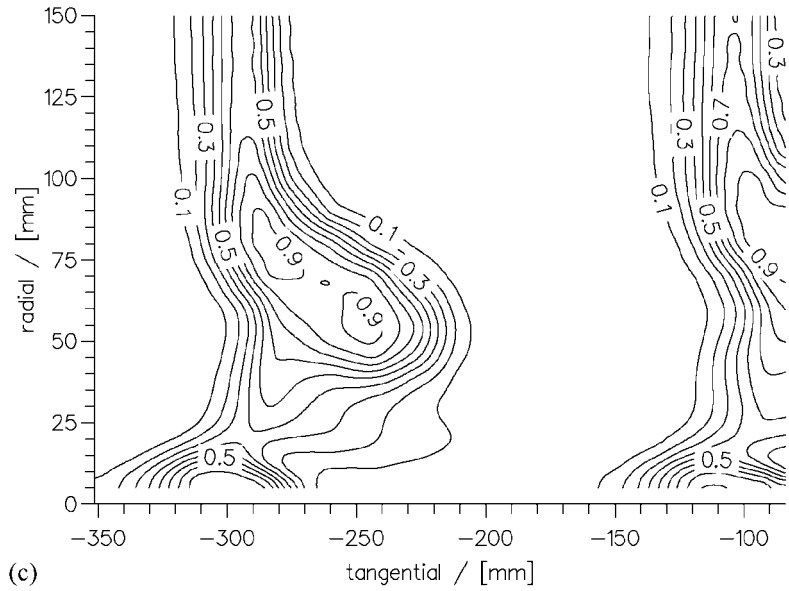

Fig. 8 Total pressure loss coefficient downstream at slot 10 for (a) planar, (b) P1 and (c) P2 profiles

contouring upstream of the leading edge has given rise to this large region which is not apparent in the planar or P2 end walls (which are planar upstream of the leading edge). A further point of note is that the HSV is much weakened by the presence of the contouring. The rising end wall on the pressure side of the leading edge perhaps expands the vortex, thus reducing its intensity.

An important result is that, although P1 and P2 have in general a very similar reduction in the passage vortex strength, P2 does not show such a great reduction in loss. Figure 9 indicates that the loss core for P2 is larger than for P1, although P2 does gain nearer the wall owing to the reduction in the countervortex strength. The traditional correlations for secondary loss have an implicit link with the strength of the passage vortex, and intuitively they might be expected to be closely linked. The reason for this disparity is not clear. One possibility is that the rapid change in curvature near the pressure side of the leading edge with P2 might induce some sort of separation. However, apart from some tenuous evidence from the tuft studies carried out by Jayaraman [**15**], there is no confirmation of this idea. At this stage all that can be said is that the process of generation of secondary loss is (not surprisingly) very complex and that it appears that restricting the profiling to within the blade passage reduces its effectiveness somewhat. Clearly further investigation is required to elucidate this problem.

The comparison of yaw angles with the CFD pre-

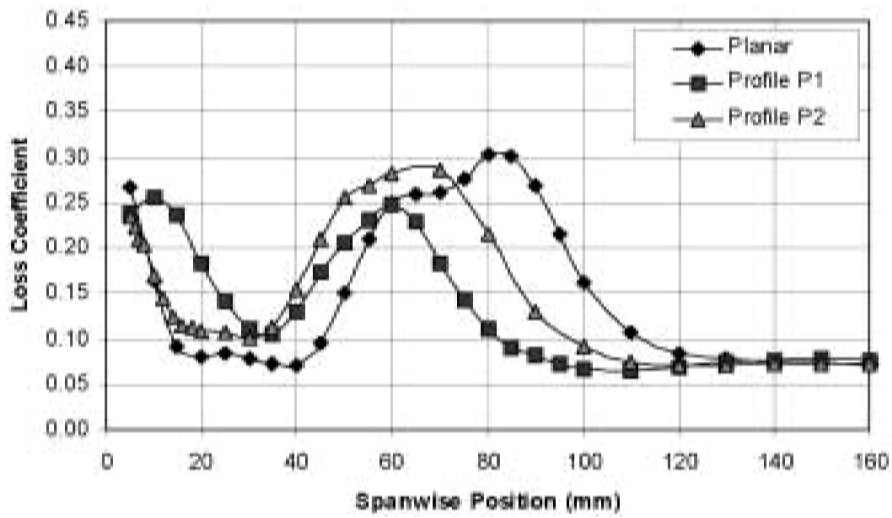

Fig. 9 Pitch-averaged total pressure loss

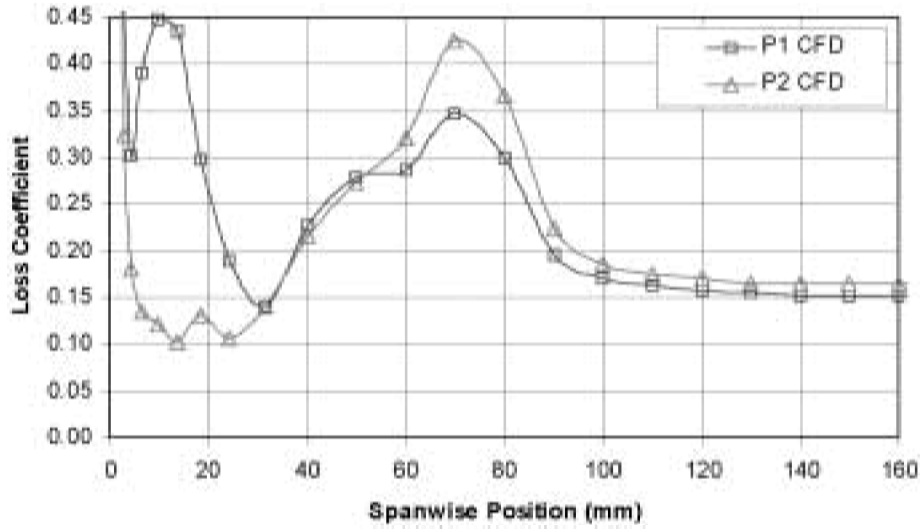

Fig. 10 CFD pitch-averaged loss

diction shows good agreement in the region of the passage vortex when a 1.5° offset is allowed for. The agreement is less good within 30 mm of the end wall. The P1 prediction showed a fall in overturning, consistent with the strong countervortex, and for the P2 prediction there is strong overturning. Neither of these features is shown by the measurements, although it should be noted that the experimental results closer to the wall than 10 mm may be in error owing to wall interference effects, since the probe was ~5 mm in diameter.

The comparison of the CFD for the pitch-averaged loss also shows good qualitative agreement in the region of the passage vortex. The mid-span error is typical of many fully turbulent computations of this blade (see reference [**17**]). The larger loss core for P2 is predicted as seen in the experiments. However, near the end wall the agreement is much poorer. The flow near the end walls is very complex and is strongly affected by viscous and turbulence effects. It is known that for the planar case there are significant regions of laminar flow on the end wall and suction surface (see reference [**18**]) and the profiling may well affect these. The CFD was carried out as fully turbulent, so it is not surprising that the CFD and experiments do not agree well near the end wall and that the prediction of loss is not reliable.

5 CONCLUSIONS

The following conclusions are drawn from this work:

1. A new profile has been designed, manufactured and tested which restricts profiling to the blade passage.
2. This new design has significantly different static pressures on the end wall.

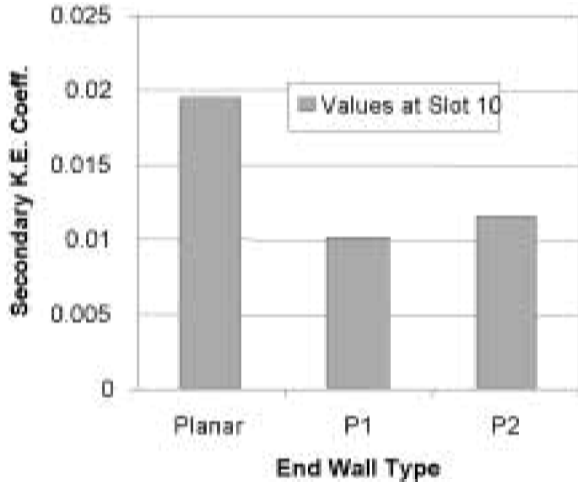

Fig. 11 Secondary kinetic energy at slot 10

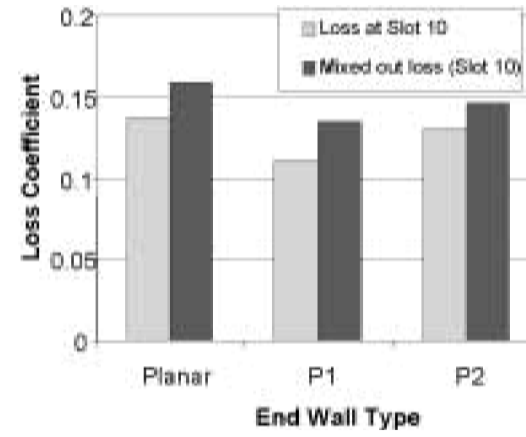

Fig. 12 Net loss values at slot 10

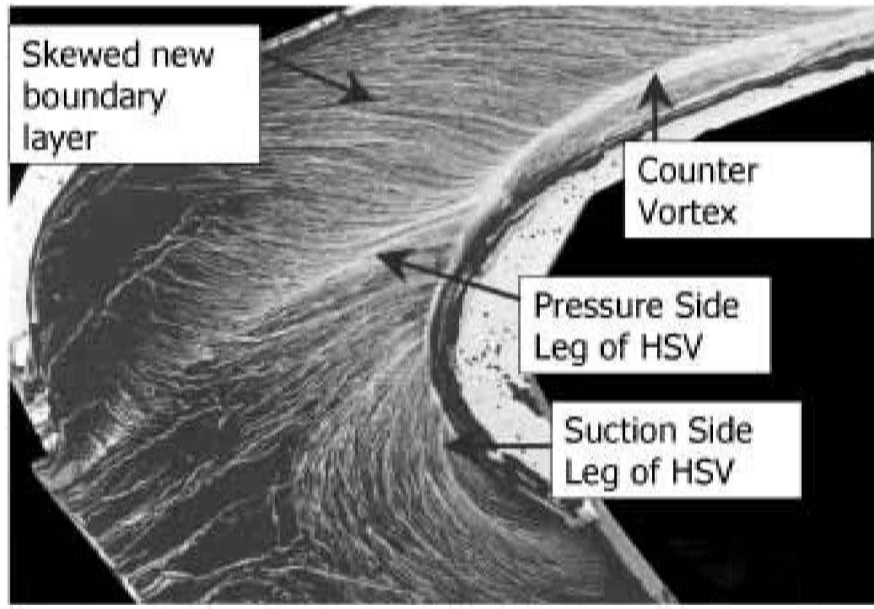

Fig. 13 Planar end wall

3. The new profile shows a similar reduction in the strength of the secondary flow.
4. The new profile does produce better exit angle deviations than the original profile, which was the design intent. However, the new profile does not produce the same level of loss reduction as the old one.
5. Flow visualization does not point to any large-scale separation which could explain this additional loss.
6. The CFD predictions, which are the basis of the design method, agree well with the experiments with respect to the flow in the passage vortex and loss core region. In particular they predict more loss in the loss core for P2 than for P1. However, the predictions nearer the end walls are less good, and this may be due to the complex transitional nature of the flow that is not modelled by the CFD.

Overall this work confirms the validity of the inverse design method with respect to the flow field predictions. However, at present CFD methods are not sufficiently accurate to predict loss with certainty. Thus, basing the design on reducing secondary flow strength and angle

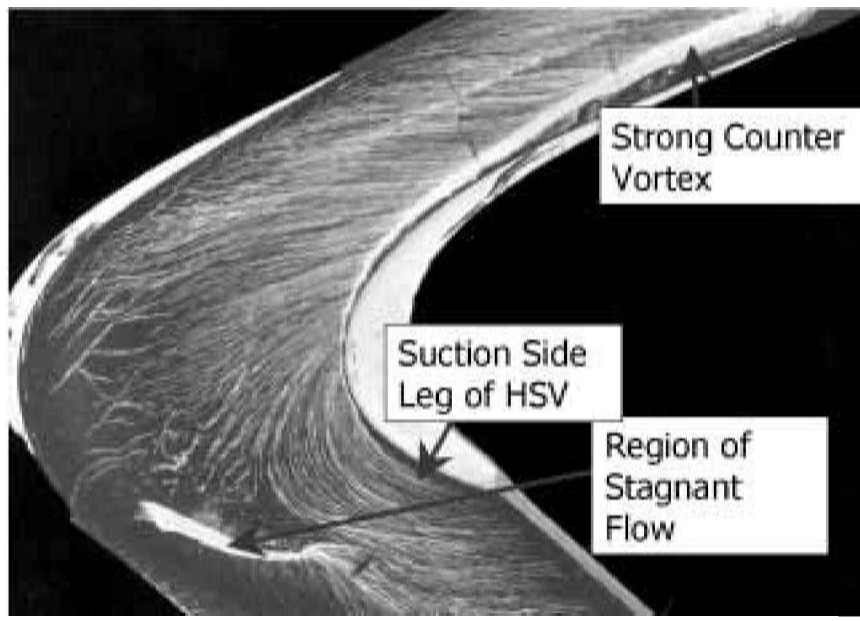

Fig. 14 Profiled end wall P1

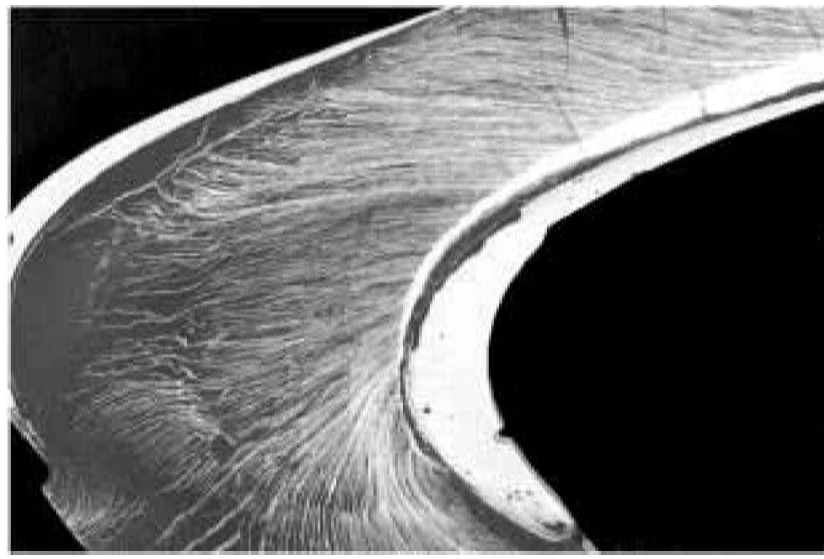

Fig. 15 Profiled end wall P2

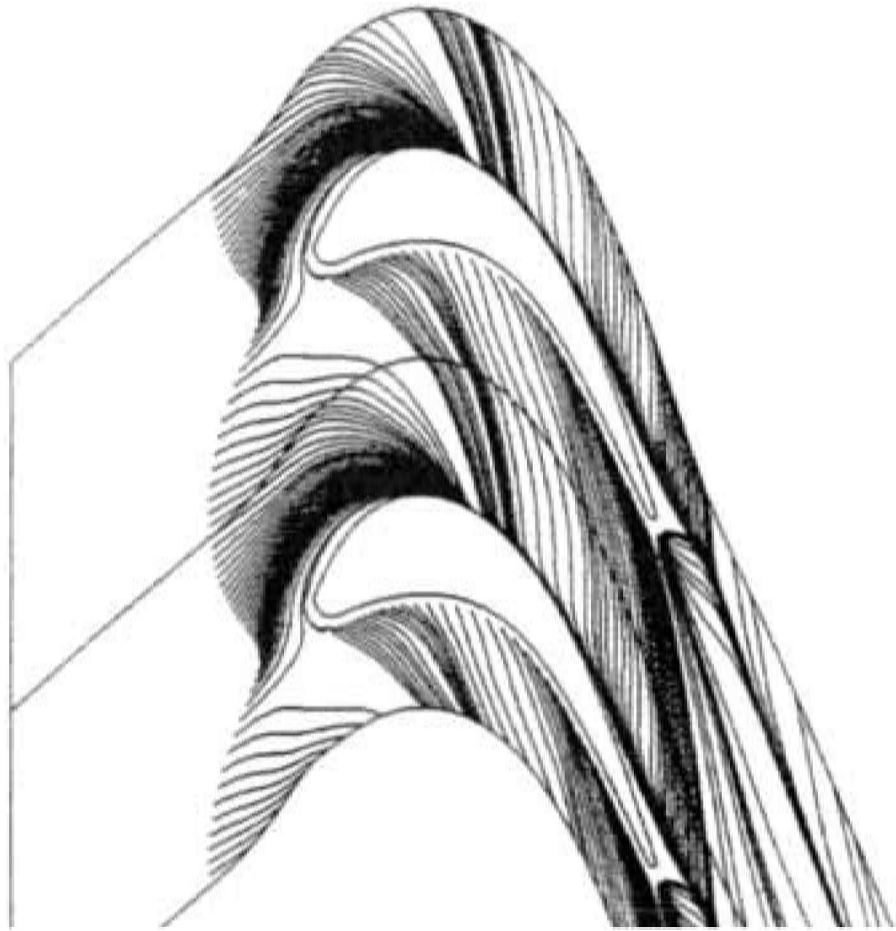

Fig. 16 CFD for profiled end wall P1

deviations is what has to be done at present. In the longer term accurate loss prediction would be desirable, but until better turbulence and transition modelling is available, the loss confirmation has to rely on experimental investigation. A final point is that the reduced secondary flow strength and deviation at the blade row exit may result in a 'cleaner' flow for a subsequent blade row, thus giving increased efficiency in that row that is not evident from this isolated blade cascade study.

ACKNOWLEDGEMENTS

This work has been carried out with the support of Rolls–Royce plc and the Defence Evaluation and Research Agency (MoD and DTI), Pyestock. The authors would like to thank them for funding it and their permission to publish this paper.

REFERENCES

1 **Sieverding, C. H.** Recent progress in the understanding of basic aspects of secondary flows in turbine blade passages. *Trans. ASME, J. Engng Gas Turbines Pwr*, 1985, **107**, 248–252.

2 **Harrison, S.** Secondary loss generation in a linear cascade of high-turning turbine blades. ASME paper 89-GT-47, 1989.

3 **Deich, M. E., Zaryankin, A. E., Filippov, G. A.** and **Zatsepin, M. F.** Method of increasing the efficiency of turbine stages with short blades. Translation 2816, AEI (Manchester) Limited, 1960 (*Teploenergetika*, February 1960, (2), 18–24).

4 **Morris, A. W. H.** and **Hoare, R. G.** Secondary loss measurements in a cascade of turbine blades with meridional wall profiling. ASME paper 75-WA/GT-13, 1975.

5 **Ewen, J. S., Huber, F. W.** and **Mitchell, J. P.** Investigation of the aerodynamic performance of small axial turbines. *J. Engng Pwr*, 1973, **95**, 326–332.

6 **Boletis, E.** Effect of tip endwall contouring on the three dimensional flow-field in an annular turbine nozzle guide vane: part 1—experimental investigation. *J. Engng Gas Turbines Pwr*, 1985, **107**, 983–990.

7 **Atkins, M. J.** Secondary losses and endwall profiling in a turbine cascade. In Proceedings of IMechE Conference, 1987, paper C255/87 pp. 29–42.

8 **Rose, M. G.** Non-axisymmetric endwall profiling in the HP NGVs of an axial flow gas turbine. ASME paper 94-GT-249, 1994.

9 **Hartland, J. C., Gregory-Smith, D. G.** and **Rose, M. G.** Non-axisymmetric end wall profiling in a turbine rotor blade. ASME paper 98-GT-525, 1998.

10 **Yan, P. J., Gregory-Smith, D. G.** and **Walker, P. J.** Secondary flow reduction in a nozzle guide vane cascade by non-axisymmetric end-wall profiling. ASME paper 99-GT-339, 1999.

11 **Harvey, N. W., Rose, M. G., Shahpar, S., Taylor, M. D., Hartland, J.** and **Gregory-Smith, D. G.** Non-axisymmetric turbine end wall design: part I. Three-dimensional design system. *J. Turbomachinery*, 2000, **122**, 278–285; also ASME paper 99-GT-337, 1999.

12 **Moore, J. G.** Calculation of 3D flow without numerical mixing. In AGARD-LS-140, 1985, pp. 8.1–8.14.

13 **Hartland, J., Gregory-Smith, D. G., Harvey, N. W.** and **Rose, M. G.** Non-axisymmetric end wall design: part II. Experimental validation. *J. Turbomachinery*, 2000, **122**, 286–293; also ASME paper 99-GT-338, 1999.

14 **Gregory-Smith, D. G.** and **Cleak, J. G. E.** Secondary flow measurements in a turbine cascade with high inlet turbulence. *J. Turbomachinery*, 1992, **114**, 173–183; also ASME paper 90-GT-20, 1990.

15 **Jayaraman, P.** An investigation of secondary flow in a turbine blade with end wall profiling. MSc thesis, University of Durham, 2000.

16 **Cleak, J. G. E.** Validation of viscous, three-dimensional flow calculations in an axial turbine cascade. PhD thesis, University of Durham, 1989.

17 **Gregory-Smith, D. G.** Calculations of the secondary flow in a turbine cascade. In International Symposium on *Computational Fluid Dynamics in Aeropropulsion*, ASME International ME'95 Congress and Exposition, AD-Vol. 49, 1995.

18 **Moore, H.** and **Gregory-Smith, D. G.** Transition effects on secondary flows in a turbine cascade. ASME paper 96-GT-100, 1996.